**RESEARCH PAPER**

# Effects of initial static shear stress on cyclic behaviour of sand stabilised with colloidal silica

Giovanni Ciardi[1] · Claudia Madiai[2]

## Abstract

Colloidal silica (CS) grouting is a soil improvement technique introduced as an innovative remedial measure against seismic liquefaction. It consists of injecting soils with a time-hardening, nanosilica-based solution forming a silica gel among soil particles. This paper presents the results of an experimental study on the effects of an initial static shear stress on the behaviour of a cyclically loaded clean sand stabilised with 5% CS. Undrained cyclic triaxial tests were performed to analyse the cyclic response of loose untreated and stabilised sand specimens, isotropically or anisotropically consolidated at the same initial mean effective stress. The consolidation stage was used to provide insight on the compressibility of stabilised soil. Stress–strain behaviour, pore water pressure response and cyclic shear resistance were investigated. The results showed that: (i) stabilised sand exhibits higher compressibility than the untreated one during isotropic consolidation; (ii) cyclic strength is higher for stabilised sand than for the untreated one, increasing as the degree of anisotropic initial stress increases; and (iii) extra pore water pressure development does not depend on the degree of initial anisotropy for stabilised sand, while the same does not hold for untreated sand. Simplified relationships are proposed to describe the consolidation process and the residual extra pore water pressure build-up process.

**Keywords** Anisotropy · Colloidal silica · Compressibility · Laboratory tests · Liquefaction · Soil stabilisation

**Abbreviations**

| | |
|---|---|
| $B$ | Skempton's pore pressure coefficient |
| $CRR_{15}$ | Cyclic resistance ratio |
| CS | Colloidal silica |
| $CS_W$ | Colloidal silica content (by weight) |
| $CSR$ | Cyclic stress ratio |
| $CSR*$ | Equivalent cyclic stress ratio |
| $D_{50}$ | Mean particle diameter |
| $D_r$ | Relative density |
| $e_{max}$ | Maximum void ratio |
| $e_{min}$ | Minimum void ratio |
| $G_s$ | Specific gravity |
| ID | Test identification number |
| $K_c$ | Consolidation stress ratio |
| $k$ | Hydraulic conductivity |
| $N$ | Number of loading cycles |
| $N_f$ | Number of loading cycles at failure |
| $p'$ | Mean effective stress |
| $p_0'$ | Initial mean effective stress |
| $q$ | Deviatoric stress |
| $q_{cyc}$ | Cyclic deviatoric stress |
| $q_{st}$ | Static deviatoric stress |
| $RPWP$ | Residual pore water pressure ratio |
| $r_u$ | Pore water pressure ratio |
| $t$ | Time |
| $U$ | Consolidation ratio |
| $U_c$ | Uniformity coefficient |
| $\Delta u$ | Extra pore water pressure |
| $\varepsilon_a$ | Axial strain |
| $\varepsilon_{DA}$ | Double amplitude axial strain |
| $\varepsilon_{DA,f}$ | Double amplitude axial strain at failure |
| $\varepsilon_v$ | Volumetric strain |
| $\varepsilon_{v,max}$ | Maximum volumetric strain |
| $\sigma'_a$ | Major principal effective stress |
| $\sigma'_r$ | Minor principal effective stress |

✉ Giovanni Ciardi
   giovanni.ciardi@unipg.it

1   Department of Civil and Environmental Engineering, University of Perugia, Via G. Duranti 93, 06125 Perugia, Italy

2   Department of Civil and Environmental Engineering, University of Florence, Via di S. Marta 3, 50139 Florence, Italy

∕ Springer

# 1 Introduction

Seismic liquefaction is considered one of the most critical phenomena that can involve soils during earthquakes. It may arise in saturated sandy/silty-sandy soils when subjected to cyclic loading due to the reduction of soil strength and stiffness caused by the development and build-up of pore water pressure [e.g. 16, 19, 22, 37]; typical consequences of seismic soil liquefaction are the loss of bearing capacity, earthen structures failures, slope failures, lateral spreading, landslides and increased lateral pressure on retaining walls.

In the framework of the liquefaction mitigation techniques, the so-called *passive site remediation* by means of colloidal silica (CS) grouting has been proposed as a method to improve the liquefaction resistance of liquefiable soils inducing minimal disturbance to the existing overlying structures [8]. This technique consists of injecting a low-viscosity, time-hardening nanosilica-based mixture by means of low injection pressure (e.g. by natural or augmented groundwater flow). This mixture becomes a silica gel after a certain time; once gelled among the soil grains, the gel modifies the soil mechanical response, increasing the liquefaction resistance of the stabilised soil [4, 6, 11]. The main features of colloidal silica grouting, inferred from the relevant literature, can be summarised as follows:

1. the initial viscosity of the CS grout can be controlled and kept as low as that of water [1, 10], facilitating the grout injection and permeation processes. Thus, colloidal silica grouting is feasible when the use of some standard liquefaction mitigation techniques (e.g. densification, blasting) would be limited by negative side-effects (i.e. induced deformation/vibrations) [e.g. 34, 43];
2. the soil stabilised by CS exhibits increased shear strength under monotonic loading conditions. The unconfined compressive strength values of the stabilised soil increase with samples' age (sometimes referred to as curing time, namely the time between the end of specimens' preparation and the beginning of the test) and silica content (namely, the percentage of silica solids diluted in the stabilising grout) [11, 13, 26, 59], generally showing an increased dilative behaviour associated with higher peak shear stress at failure [21, 29, 32, 35, 44];
3. the stabilised soil is more compressible than the untreated one, and both the CS liquid and the CS gel are more compressible than water [42, 47]: the enhanced compressibility of the stabilised soil has been consistently observed in laboratory under both oedometric and isotropic compression [3, 13, 29, 43, 44];
4. the liquefaction resistance of the stabilised soil increases with increasing silica content and curing time [3, 6, 11, 21, 31, 43, 47];
5. the failure condition of the stabilised soil during cyclic loading seems not to be related to the pore water pressure development and build-up [9, 29, 31];
6. in situ applications of CS grouting have been successfully performed, showing its feasibility at the field-scale [9, 34].

Although laboratory investigations have been thoroughly carried out to analyse the cyclic response of soils stabilised by CS, none of the experimental studies deals with the effects of anisotropic initial stress on the cyclic behaviour of stabilised sand [4]. On the other hand, in most in situ conditions a soil element is subjected to an initial anisotropic stress state [49, 55, 57]. In laboratory, this state can be reproduced in anisotropically consolidated specimens: in cyclic triaxial tests, specimens are subjected to a nonzero deviatoric stress, applied before the cyclic stage, resulting in a static shear stress of given magnitude acting on the maximum shear stress plane. The presence of the static shear stress makes the cyclic loading not symmetrical about the hydrostatic state; this can result, in untreated soil specimens, in distinctive deformation patterns and failure modes depending, among other factors, on the magnitude of the applied static shear stress, on the initial confining stress, on the relative density, on the degree of stress-reversal, as well as on the specimen formation method [e.g. 41, 51, 54, 55, 57]. These factors also influence the residual pore water pressure generated during cyclic loading that can reach a limiting value also depending on the initial anisotropic stress level [28, 45, 58].

Anisotropically consolidated specimens can yield, under similar conditions, significant differences in the cyclic behaviour and in the cyclic strength [15, 25, 45, 49, 54]: previous laboratory investigations on untreated soil showed that the presence of an initial static shear stress can be beneficial or detrimental for the soil liquefaction resistance [41, 45, 49, 54, 55, 57, 60]. While many studies evaluate the effects of the initial static shear stress on the cyclic behaviour of untreated sands, no data are available on the effects of the initial static shear stress on the cyclic response of sands stabilised by CS. Thus, the main purpose of this paper is to start filling the gap on this topic. In this perspective, laboratory investigations were carried out. Varying the degree of anisotropic initial stress, undrained cyclic triaxial tests were performed on untreated and stabilised (by 5% CS grout, by weight) clean sand specimens. After describing the used materials, the specimens' formation methods and the test set-up, the test results are presented and discussed. The isotropic consolidation stage was also used to get more information about the compressibility properties of the stabilised soil. The cyclic response is shown to be dependent on the degree of initial anisotropy, with distinctive features belonging to untreated

and stabilised sand. Simplified relationships are proposed to describe the consolidation process and the residual pore water pressure build-up process.

## 2 Experimental program

### 2.1 Materials and equipment

#### 2.1.1 Sand

The material used in this research is a clean, uniform, mainly siliceous sand, named S3 sand. This sand, made of sub-rounded, low-sphericity grains, is classified as SP material (Unified Soil Classification System). It has specific gravity $G_s = 2.65$, mean particle diameter $D_{50} = 0.30$ mm, uniformity coefficient $U_c = 1.6$, and maximum and minimum void ratio $e_{max} = 0.839$ and $e_{min} = 0.559$ [7], respectively. The grain size distribution curve of the tested sand is shown in Fig. 1.

#### 2.1.2 Colloidal silica

Colloidal silica is a suspension of silica particles of colloidal size (ranging from 1 up to 100 nm) into a liquid phase. It is obtained from saturated solutions of silicic acid ($H_4SiO_4$) and it is a harmless, stable, not pollutant, chemically and biologically inert fluid [14, 17]. CS is commercially available with different given silica contents. According to Whang [50], the expected lifetime of CS is more than 25 years, while according to Gallagher et al. [12] the material cost, when diluted at 5% by weight, could be comparable to that of microfine cement.

The CS mixture can form a silica gel if the repulsive forces acting among silica solids are decreased, thus forcing silica particles to coalesce and aggregate. To activate the gel formation process, the ion concentration (ionic strength), the silica content, the pH and the temperature of the grouting solution can be adjusted in a controlled manner [1, 11, 17]. For the purposes of geotechnical engineering, the easiest and most common way to trigger the gelation reaction is to adjust the ionic strength of the CS suspension by adding an electrolyte (i.e. a salt-based solution).

MasterRoc® MP 325 (BASF SE) was used in this study as the colloidal silica product: it consists of a clear solution with $15 \pm 1\%$ (by weight) silica content, density of $\approx 1.1$ kg/L (20 °C), viscosity of $\approx 10$ mPa s (20 °C) and pH of $10 \pm 1$ (20 °C). To obtain the formation of the CS gel, a sodium chloride (NaCl) solution (consisting of NaCl powder mixed with demineralised water with ratio 1:10 by weight) was used. The stabilising mixture, here referred to as (CS) grout and used for soil treatment, was made of distilled water, MasterRoc® MP 325 and NaCl solution mixed at fixed ratios, depending on the required gel time and silica content (herein intended as the percentage of silica particles diluted in the grout, by weight, and indicated as $CS_W$ in the following). All experiments were carried out at room temperature (20 ± 1 °C).
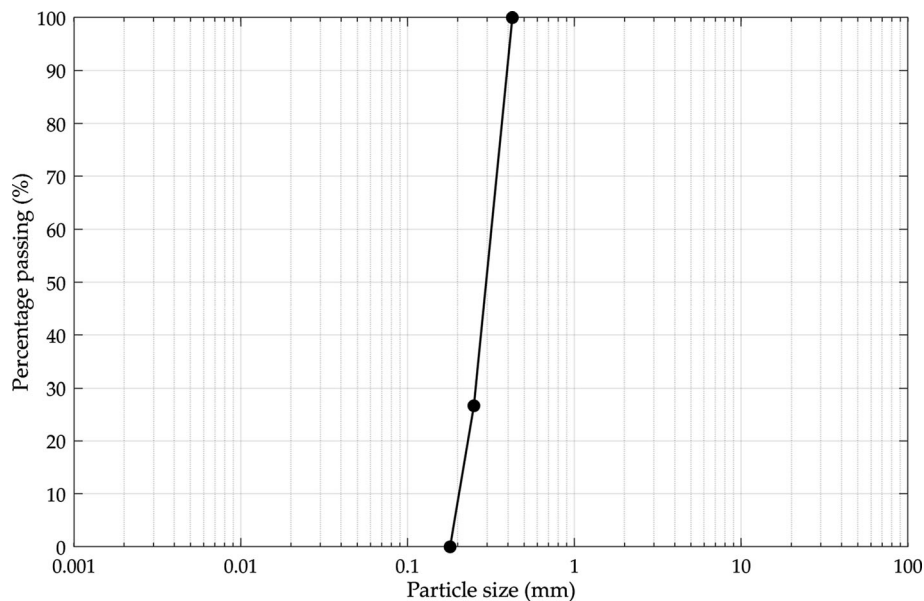


**Fig. 1** Particle size distribution of the tested sand

### 2.1.3 Triaxial apparatus

Stress-controlled undrained cyclic triaxial tests were performed using an automated electro-mechanical triaxial apparatus (Controls), capable of performing different functions, including isotropic/anisotropic consolidation, as well as applying different loading modes, such as regular or user-defined waveforms.

## 2.2 Samples' preparation and saturation

### 2.2.1 Overview

Cylindrical specimens $\approx 50/100$ mm diameter/height were subjected to cyclic triaxial tests. The moist tamping technique was used for the preparation of both untreated and stabilised samples: in the latter case, a specific triaxial-like apparatus (see Sect. 2.2.3) was used for specimens' formation, pre-saturation and for the CS grout injection before moving the samples into the triaxial cell.

It is worth reminding that different specimens' formation methods (e.g. moist tamping, water pluviation, air pluviation, etc.) can produce distinctive fabrics; thus, specimens of the same material prepared by different techniques can yield significantly different soil properties under the same testing conditions [23, 27, 56]. Therefore, it should be kept in mind that the findings of this study are related to the method used for specimens' reconstitution.

In the moist tamping method used in this study, the material was placed in layers into a cylindrical split-mould with a latex membrane stretched along its walls and compacted to achieve the desired initial void ratio. For each layer, a fixed weight of oven-dried sand was premixed with 5% distilled and deaired water and compacted with a tamper; the top of each layer was gently scarified before the following layer was put in place. To compensate for the effect of further densification induced by tamping on lower layers, and therefore to achieve a uniform mean initial void ratio within the sample, an undercompaction technique was adopted [24, 26]: each layer was prepared to a target relative density increasing of 1% from the bottom to the top of the specimen, with the middle layer prepared at the target initial void ratio. All specimens were prepared to a nominal (namely, initial) target relative density $D_r \approx 30\%$, calculated from the samples' dimensions measured before each test was run.

After preparation, both untreated and stabilised samples were saturated in the triaxial cell with distilled and deaired water before they were isotropically/anisotropically consolidated; the actual $D_r$ (namely, after consolidation) was calculated for all saturated samples, treated and untreated, from the measurements of water volume change at the end of the consolidation process.

In some previous studies, no back pressure was used to saturate the specimens stabilised by CS prior to shearing, as not to disturb the gel structure (e.g. [3, 11, 47]). Recently published data pointed out that repeatable results were obtained from drained triaxial tests when the back pressure was varied in the range 300–700 kPa, suggesting that no disturbance to the gel was provided [29, 44]. Therefore, in this study, the specimen saturation was achieved by increasing both cell and back pressure by steps (the latter with maximum value of 350 kPa), maintaining $\approx 10$ kPa effective stress during this phase. The saturation phase lasted about 24 h and it was considered complete if Skempton's coefficient $B$ was greater than 0.95.

### 2.2.2 Untreated samples

Untreated sand samples were formed directly on the triaxial base: a small vacuum (20 kPa) was applied to sustain the samples during the assembly of the triaxial apparatus and then removed: as the cell pressure increased, the applied vacuum decreased by the same amount. In this way, the initial effective stress state (and thus the initial $D_r$) did not change due to vacuum release. Carbon dioxide was then percolated under a cell pressure of 20 kPa for about 30 min before the samples were flushed with distilled and deaired water, to facilitate air removal. A conventional back-pressure saturation stage followed. $B$-check revealed $B \geq 0.98$ for all samples after one night saturation.

### 2.2.3 Stabilised samples

In previous experimental investigations on sands stabilised by CS, different techniques have been used to prepare samples for cyclic/monotonic triaxial testing. The most used techniques are: (1) the pluviation of dry sand into liquid grout [3, 11, 13, 44] and (2) the preparation of samples in standard ways (e.g. dry sand deposition, dry/-moist tamping) followed by grout injection [31, 35, 47]. Specimens prepared according to method 1 are characterised by a uniform grout distribution within the soil sample; however, the pluviation technique is not representative of field injection. On the contrary, even if the treatment homogeneity may be questionable for samples prepared according to method 2, this one simulates more accurately than method 1 the process of grout injection/penetration through the porous medium, where complete full gel-saturation is not guaranteed. This is a key issue for practical applications of CS grouting, and for this reason method 2 was adopted in this study. As discussed in Sect. 3.1, the adopted procedure led to reproducible results, thus indicating the good quality of the tested samples.

In order to prevent the drainage lines and pressure transducers of the triaxial cell from clogging by the CS gel,

stabilised sand samples were prepared in a specific triaxial-like apparatus and then moved to the triaxial cell at the age of testing. This triaxial-like device, with slight modifications, was used in a previous study for hydraulic conductivity measurements in untreated and stabilised sand samples [3] and it consists of a PVC pedestal, a plexiglass cell and a 50-mm perforated top cap. Like a usual triaxial apparatus, both the pedestal and the top cap are equipped with drainage lines to allow a flow of water (or grout) within the samples; moreover, the cell can be filled with water from an outside tank, allowing the application of a cell pressure by an air pressure regulator.

The specimens were prepared in two steps.

1. The sand samples were reconstituted by the moist tamping technique, and the triaxial-like apparatus was assembled; the vacuum removal, carbon dioxide and distilled and deaired water flushing were identical to those described in Sect. 2.2.2. At the end of this step, hydraulic conductivity measurements were taken in falling head mode. The hydraulic conductivity ($k$) was measured in the range $1.2–3.9 \cdot 10^{-3}$ m/s, typical values of medium and fine sands with grain size between 0.1 and 0.5 mm and void ratios between 0.6 and 0.8 [20]. Such a narrow range of the $k$ values was considered a satisfying indicator of the samples' quality before CS grout injection.

2. CS grout injection followed: a 500 mL CS grout solution was prepared into an external plexiglass reservoir connected to the bottom drainage line on the base and, eventually, the CS grout was permeated through the samples at atmospheric pressure, from the bottom to the top, under hydraulic gradients $\leq$ 1.6, in falling head mode. The gel time and $CS_W$ of the mixture were set in $\approx$ 24 h and 5%, respectively. The injection phase was considered complete once $\approx$ 440 mL of grout, corresponding to $\approx$6 times the specimens' volume of voids, was collected at the outer drainage. The average time for grout injection was $\approx$ 3 min. After the injection, the drainage valves were closed, and the specimens were left to cure in the cell. At the age of testing, the samples were carefully removed from the device and then put on the triaxial pedestal, with water-saturated porous stones and wet filter paper at the top and at the bottom.

Even though the gel strength continues to increase over time (e.g. Yonekura and Miwa [59] found that the unconfined compressive strength of samples was still increasing after almost three years), there is no standard procedure to select curing time for laboratory tests: this is usually taken as a multiple of the gel time, varying from units to hundreds of times the gel time (e.g. [11, 29, 47]), which usually ranges from minutes to days [1, 6]. In this study,

5 days, corresponding to 5 times the gel time, were chosen as the standard curing time before starting the cyclic stage of the test (4 days if one considers the beginning of the water-saturation stage in the triaxial cell).

Some degree of specimens' disturbance was expected due to the unloading (removal of the 20 kPa confining pressure during the disassembling of the triaxial-like apparatus) and the following moving of the samples to the triaxial pedestal after curing time had expired (e.g. [48]). A disturbance assessment was undertaken by measuring samples' sizes before grouting (at the beginning of step 1) and after the placement on the base platen of the triaxial cell. For all tested samples, this difference in dimensions was well < 0.1%, thus indicating that minimal disturbance occurred during this process. The samples' dimensions recorded after placement on the triaxial base were used for the nominal $D_r$ assessment; the triaxial cell was finally assembled.

A conventional back-pressure water-saturation phase followed; B-check revealed B $\geq$ 0.96 for all samples after one night saturation. Figure 2 shows a scheme of the triaxial-like system used for preparation and grouting of the stabilised samples.

## 2.3 Isotropic and anisotropic consolidation

At the end of the saturation phase, all specimens were isotropically consolidated to the same initial mean effective stress $p_0' = (\sigma_a' + 2\sigma_r')/3 = 100$ kPa, where $\sigma_a'$ and $\sigma_r'$ are the major and minor principal effective stresses during the consolidation stage, respectively. In the case of anisotropic consolidation, a static shear stress ($q_{st}$) was applied after the isotropic consolidation stage by applying a deviatoric stress (namely, $q_{st} = \sigma_a' - \sigma_r'$) under drained conditions and different consolidation stress ratios $K_c = \sigma_a'/\sigma_r'$. In case of isotropic consolidation, it follows that $q_{st} = 0$ kPa and $K_c = 1.0$. The same definition of anisotropic consolidation has been used in previous research [25, 39, 58]. The consolidation phase was considered complete if the pore pressure increase (if any), once the drainage valve was closed, was no more than 0.5% of $p_0'$ over 30 min. In this study, three different test series were performed with $K_c = 1.0, 1.3, 1.6$.

## 2.4 Shearing and test series

Consolidated samples were subjected to a cyclic stress applied by a sinusoidal load of given amplitude at a frequency of 0.1 Hz to have stable input and output signals, and thus reliable measurements during the tests. Depending on the magnitude of the applied cyclic deviatoric stress ($q_{cyc}$), compared to the magnitude of the initial static deviatoric stress ($q_{st}$), three different loading configurations
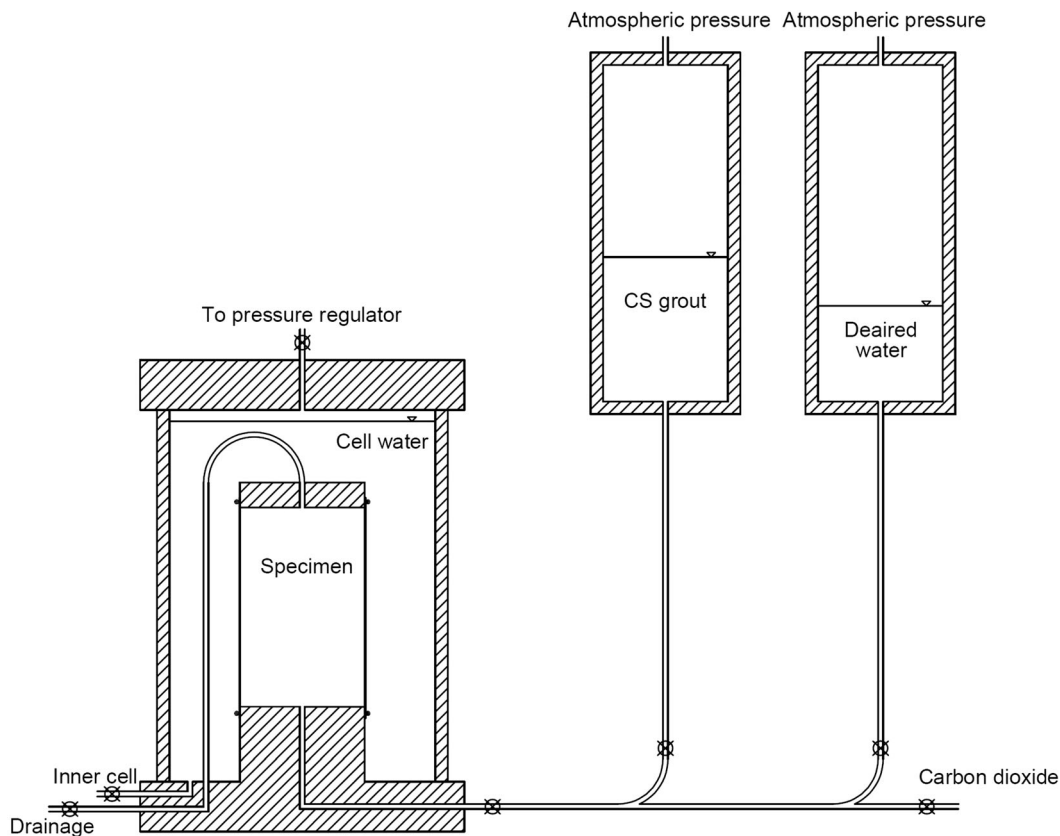
**Fig. 2** Scheme of the system used for the preparation of samples stabilised by CS (not to scale)

can be reproduced. When $q_{st}$ is zero, the application of the cyclic deviatoric stress $q_{cyc}$ is symmetrical about the zero-shear stress axis; conversely, the condition $q_{st}$ nonzero imposes non-symmetrical loading condition, produced by the application of the cyclic deviatoric stress $q_{cyc}$. If $q_{cyc} > q_{st}$, the loading is applied with stress-reversal; if $q_{cyc} < q_{st}$, the loading is applied without stress-reversal [54]. In this study, only tests with symmetrical loading and non-symmetrical loading with stress-reversal (i.e. with $q_{cyc} > q_{st}$) were carried out.

In triaxial tests on liquefiable sand (with or without a certain amount of fines), it has become customary to identify the failure condition with the occurrence of a given value (typically, 5%) of double amplitude axial strain ($\varepsilon_{DA}$): in clean, loose sand, the development of sizeable amount of cyclic strain immediately follows the initial liquefaction condition (sometimes simply referred to as "liquefaction"), namely when the excess pore water pressure ($\Delta u$) equals the initially applied confining pressure [19]. This condition corresponds to a value of the pore water pressure ratio, $r_u = \Delta u / p_0'$, equal to 1.0. However, when dealing with sand stabilised by CS, it has been observed that the pore water pressure response is somewhat different from that of the untreated soil under the same conditions, and that the stabilised soil never exhibits sand-

like collapse [21, 29, 31]. Therefore, the (initial) liquefaction does not have the same physical meaning in untreated sand and in stabilised sand, whose failure condition has therefore been defined in most of previous studies in terms of accumulated strain. In the light of these remarks, $\varepsilon_{DA} = 5\%$ was adopted as the strain threshold to coherently identify the failure for both stabilised sand and untreated sand subjected to cyclic triaxial tests; the failure is assumed to occur at a number of loading cycles at failure, $N_f$, associated with the first occurrence of $\varepsilon_{DA} \geq 5\%$.

The experimental tests performed in this study, along with the relevant main information, are summarised in Table 1, where ID is the test identification number, *CSR* (cyclic stress ratio) is the ratio of the maximum applied cyclic shear stress to the initial mean effective consolidation stress ($CSR = q_{cyc}/(2p_0')$ and $\varepsilon_{DA,f}$ is the double amplitude axial strain at failure.

## 3 Results

### 3.1 Isotropic consolidation behaviour

A "side" effect of the CS treatment (when it is used with the primary goal of liquefaction mitigation) is the reduction

**Table 1** List of undrained cyclic triaxial tests

| Series | ID | $CS_W$ (%) | $\sigma_r'$ (kPa) | $\sigma_a'$ (kPa) | $K_c$ (−) | CSR (−) | $D_r$ after consolidation (%) | $N_f$ ($\varepsilon_{DA} \geq 5\%$) (−) | $\varepsilon_{DA,f}$ (%) |
|---|---|---|---|---|---|---|---|---|---|
| 1 | 01-0 | 0 | 100 | 100 | 1.0 | 0.203 | 30 | 79 | 8.11 |
| | 02-0 | 0 | 100 | 100 | 1.0 | 0.232 | 31 | 35 | 7.81 |
| | 03-0 | 0 | 100 | 100 | 1.0 | 0.253 | 29 | 20 | 5.24 |
| | 04-0 | 0 | 100 | 100 | 1.0 | 0.303 | 31 | 4 | 9.05 |
| | 01-5 | 5 | 100 | 100 | 1.0 | 0.228 | 31 | 263 | 5.01 |
| | 02-5 | 5 | 100 | 100 | 1.0 | 0.253 | 35 | 64 | 5.04 |
| | 03-5 | 5 | 100 | 100 | 1.0 | 0.277 | 32 | 36 | 5.06 |
| | 04-5 | 5 | 100 | 100 | 1.0 | 0.302 | 31 | 13 | 5.26 |
| 2 | 05-0 | 0 | 90 | 120 | 1.3 | 0.301 | 31 | 57 | 5.10 |
| | 06-0 | 0 | 90 | 120 | 1.3 | 0.327 | 31 | 27 | 6.26 |
| | 07-0 | 0 | 90 | 120 | 1.3 | 0.352 | 32 | 18 | 6.39 |
| | 08-0 | 0 | 90 | 120 | 1.3 | 0.377 | 31 | 7 | 6.91 |
| | 05-5 | 5 | 90 | 120 | 1.3 | 0.362 | 36 | 58 | 5.04 |
| | 06-5 | 5 | 90 | 120 | 1.3 | 0.415 | 32 | 26 | 5.05 |
| | 07-5 | 5 | 90 | 120 | 1.3 | 0.460 | 32 | 17 | 5.06 |
| | 08-5 | 5 | 90 | 120 | 1.3 | 0.630 | 32 | 8 | 5.07 |
| 3 | 09-0 | 0 | 83 | 133 | 1.6 | 0.326 | 30 | 129 | 5.00 |
| | 10-0 | 0 | 83 | 133 | 1.6 | 0.352 | 32 | 54 | 5.57 |
| | 11-0 | 0 | 83 | 133 | 1.6 | 0.376 | 30 | 25 | 5.27 |
| | 12-0 | 0 | 83 | 133 | 1.6 | 0.401 | 31 | 12 | 5.83 |
| | 09-5 | 5 | 83 | 133 | 1.6 | 0.455 | 30 | 38 | 5.06 |
| | 10-5 | 5 | 83 | 133 | 1.6 | 0.505 | 34 | 20 | 5.14 |
| | 11-5 | 5 | 83 | 133 | 1.6 | 0.560 | 31 | 13 | 5.04 |
| | 12-5 | 5 | 83 | 133 | 1.6 | 0.590 | 30 | 11 | 5.19 |

of the soil hydraulic conductivity, $k$. Previous research showed that the $k$ value of the soil after stabilisation by CS was significantly lower than before the treatment. The values of $k$ for CS grouted soils fall in typical range of clay-like materials [3, 30, 32, 46] and decrease as $CS_W$ increases. By way of example, for the same kind of sand used in this study with a relative density $D_r \approx 62$–64%, $k$ values were measured in the range $2.4$–$2.6 \cdot 10^{-4}$ m/s for $CS_W = 0\%$, decreasing to $k$ values in the range $1.5$–$3.8 \cdot 10^{-9}$ m/s after stabilisation with $CS_W = 5\%$ [3]. Because of the differences in $k$ values in sand stabilised by CS and in untreated sand, the isotropic consolidation process is expected to be longer for the former material.

The experimental results are summarised in Fig. 3 in terms of both volumetric strain ($\varepsilon_v$) versus time ($t$), and average consolidation ratio ($U$) versus time; $U$ is defined as the ratio of the amount of extra pore water pressure dissipated at time t ($\Delta u(t_0) - \Delta u(t)$) to the maximum amount of extra pore pressure at the beginning of consolidation ($\Delta u(t_0)$). Plots in Fig. 3a, b show the experimental upper bound and lower bound trend of $\varepsilon_v(t)$ for untreated sand and for stabilised sand, respectively, while Fig. 3c, d shows the experimental upper bound and lower bound trend of

$U(t)$ for untreated sand and for stabilised sand, respectively. In Fig. 3a, b, $\varepsilon_v > 0$ indicates the volume contraction (water is flowing outside the specimen); consequently, the values on the $y$-axis increase downwards. For the untreated sand (Fig. 3a), $\varepsilon_v$ attains the maximum value ($\varepsilon_{v,max}$) almost immediately; the same holds for the maximum consolidation ratio (Fig. 3c) and, in this case, the upper and lower bound essentially coincide. For the sand stabilised by CS, both the volume reduction (solid grey lines in Fig. 3b) and the extra pore water pressure dissipation (solid grey lines in Fig. 3d) are delayed. Moreover, the values of $\varepsilon_{v,max}$ on stabilised soil are greater than those of untreated soil, $[\varepsilon_{v,max}(CS_W = 5\%)]_{lower\ bound} > [\varepsilon_{v,max}(CS_W = 0\%)]_{upper\ bound}$, pointing out that the stabilised sand is significantly more compressible. Thus, under the same $p_0'$, the CS gel seems to facilitate the grains' mobility, acting as a sort of buffer among soil particles [13, 44].

Based on the experimental results acquired from the isotropic consolidation process of stabilised soil specimens, the following equations are proposed for the variation of volumetric strain (Eq. 1) and average consolidation ratio (Eq. 2) with time ($t$), respectively:
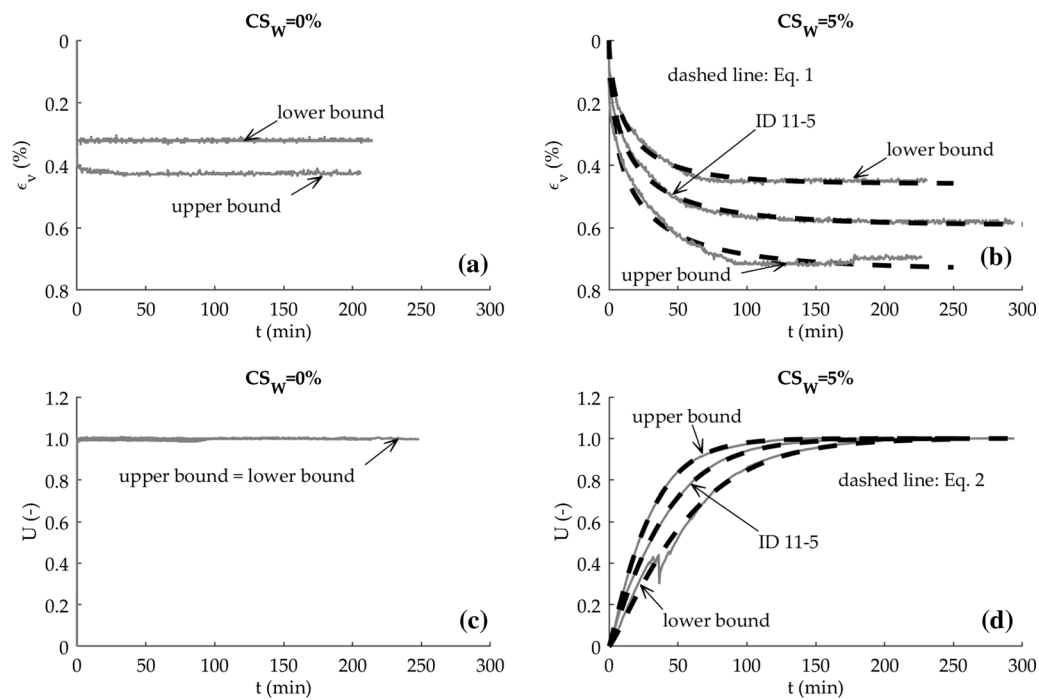
**Fig. 3** Volumetric strain ($\varepsilon_v$) and average consolidation ratio ($U$) versus time in isotropic consolidation stage: **a**, **c** untreated sand, **b**, **d** stabilised sand (experimental data in solid grey lines and curve fitting in dashed black lines)

**Table 2** Best fitting parameters for the curves shown in Fig. 3b, d

| Curve | $a$ | $b$ | $c$ | $d$ | $f$ | $R^2$ (Eq. 1) | $R^2$ (Eq. 2) |
|---|---|---|---|---|---|---|---|
| Lower bound | 0.4594 | 0.1794 | 0.6347 | 0.008068 | 1.183 | 0.978 | 0.994 |
| Upper bound | 0.7367 | 0.2400 | 0.5234 | 0.02203 | 1.124 | 0.964 | 0.999 |
| ID 11-5 | 0.5920 | 0.2080 | 0.5652 | 0.01656 | 1.108 | 0.988 | 0.999 |

$$\varepsilon_v = a \cdot \left(1 - 1/e^{b \cdot t^c}\right) \tag{1}$$

$$U = 1 - 1/e^{d \cdot t^f} \tag{2}$$

In Eqs. 1 and 2, $a$, $b$, $c$, $d$, $f$ are curve fitting parameters to be calibrated on the experimental data. For a given soil, it is likely they depend on the initial $D_r$, $CS_W$ and $p_0'$. Figure 3b, d shows the proposed models (Eqs. 1 and 2) fitted to the upper and lower bounds of the experimental results obtained on stabilised sand specimens (dashed black lines). In addition, the experimental data from test ID 11-05 and the corresponding fitting curve are also reported in Fig. 3b, d, by way of example. The best fitting parameters, together with the coefficient of determination $R^2$ for Eqs. 1 and 2, are summarised in Table 2.

The different behaviour between stabilised sand and untreated sand shown in Fig. 3 has been consistently observed for all tests performed in this study. The lower permeability of the stabilised soil slows down the dissipation of the extra pore water pressure and volumetric strain changes, while the compressibility of the gel inside the voids, together with the enhanced soil grains' mobility, causes an overall greater value of $\varepsilon_{v,max}$. A possible explanation of these results can be given following a phenomenological approach. The gel matrix itself can be viewed as a sort of soil-like structure, being composed of aggregated silica clusters (the "equivalent" to soil particles) with water dispersed in micro-pore spaces through which water can flow [40]. Consequently, a saturated CS gel volume element behaves like a water-saturated untreated soil volume element when subjected to an undrained total stress increase followed by drained conditions: the water will flow outside the volume element, with silica particles rearranging in a denser state. The stabilised soil can therefore be viewed as composed of a soil skeleton with pores filled with CS gel: when subjected to an effective stress increase, the soil grains rearrange in a denser state and, at the same time, this holds for the silica particles in the gel matrix. This process enhances the mobility of the soil grains themselves, resulting in an

overall greater volume reduction, if compared to the case of untreated water-saturated soil under the same conditions. According to the results of previous research, this enhanced grains' mobility could depend on $CS_W$: Ciardi et al. [3], analysing oedometer test results on samples with different CS contents, found that the volumetric strain exhibited by stabilised sand was always greater than that of the untreated sand; moreover, for $CS_W > 5\%$, the stress–strain curves were comparable with those for $CS_W = 5\%$. Based on this evidence, they speculated the presence of a $CS_W$ threshold above which the compressibility of stabilised soil was reduced. Towhata and Kabashima [43] showed that the volumetric strain of sand specimens stabilised by CS during isotropic consolidation in triaxial cell was greater than that exhibited by the untreated sand. In addition, they found that specimens stabilised by 4.5% silica showed a higher compressibility than sand stabilised by 6.5% silica. For high CS content (34%), Wong et al. [52] found that the compressibility of stabilised soil samples in oedometer tests was lower than that of the untreated ones.

## 3.2 Cyclic behaviour and failure mechanisms

Figures 4, 5, 6, 7, 8 and 9 show typical results from the cyclic shear stage of undrained triaxial tests on untreated sand and on stabilised sand under different $K_c$ values in terms of: mean effective stress $p'$ versus deviatoric stress $q$; axial strain $\varepsilon_a$ versus $q$; number of loading cycles $N$ against $r_u$ and $N$ against $\varepsilon_a$. The obtained results are discussed in detail in the following paragraphs.

### 3.2.1 Isotropic initial stress conditions

Figures 4 and 5 show the experimental results on untreated sand and on stabilised sand, respectively, under the same $CSR = 0.253$ and consolidation conditions (isotropic state, $K_c = 1.0$). As shown in Fig. 4 for the untreated sand, $p'$ decreases continuously as the pore pressure develops. In the proximity of the initial liquefaction, the axial strain starts growing significantly, and once the condition $r_u = 1.0$ ($p' = 0$ kPa) is reached ($N = 19.1$), $\varepsilon_a$ increases dramatically ($\varepsilon_{DA} = 2.31\%$ for N = 19, rising to 5.24% for $N = 20$ and to 9.72% for $N = 21$) identifying a state of softening for the untreated material. According to the adopted failure criterion (Sect. 2.4), the number of loading cycles at failure in this test is $N_f = 20$. For the stabilised soil specimen, the stress paths and deformation patterns are substantially different (Fig. 5). Like for the untreated sand, $p'$ decreases as $r_u$ increases: in this case, however, the initial liquefaction condition ($r_u = 1.0$ for $N = 51.2$) does not produce a sudden development of axial strain, and the material can be stressed by many more loading cycles before 5% DA axial strain is developed ($\varepsilon_{DA} = 5.04\%$ for $N_f = 64$). It is observed that $\varepsilon_a$ is not symmetric about the zero-strain axis and that it gradually develops mainly to the extension zone [11, 31]. The rate at which $r_u$ increases is faster for the stabilised sand than for the untreated one [29, 31]: by way of example, for the stabilised sand $r_u = 0.8$ for $N = 12.2$ (Fig. 5c), occurring after $\approx 19\%$ of $N_f$, while for the untreated sand (Fig. 4c) $r_u = 0.8$ for $N = 18.1$, corresponding to $\approx 90\%$ of $N_f$. Finally, by
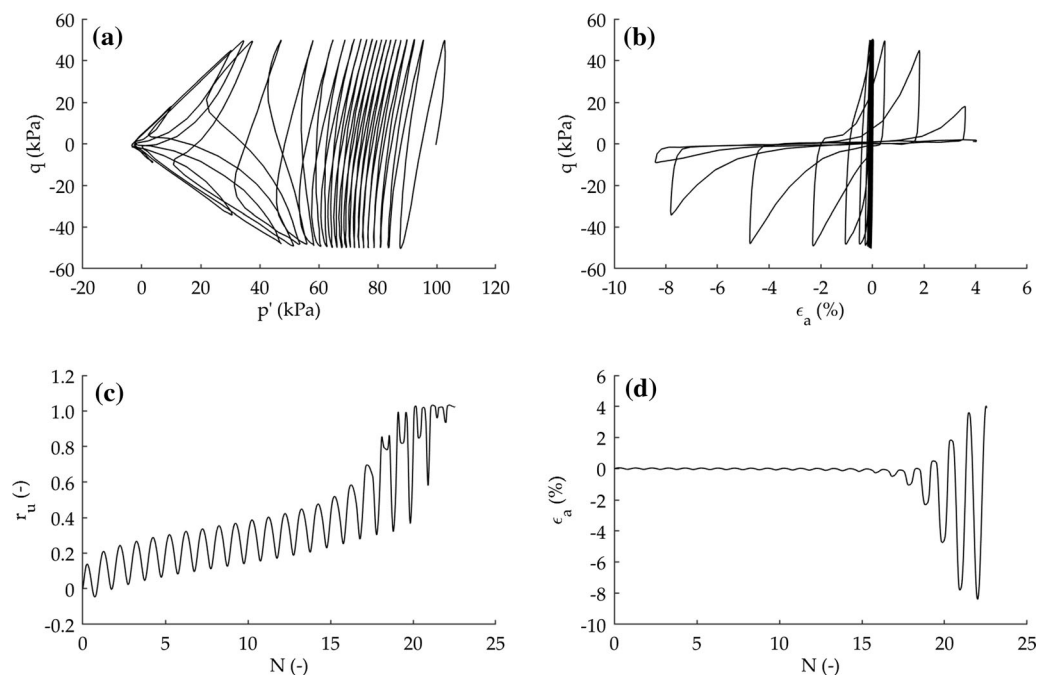


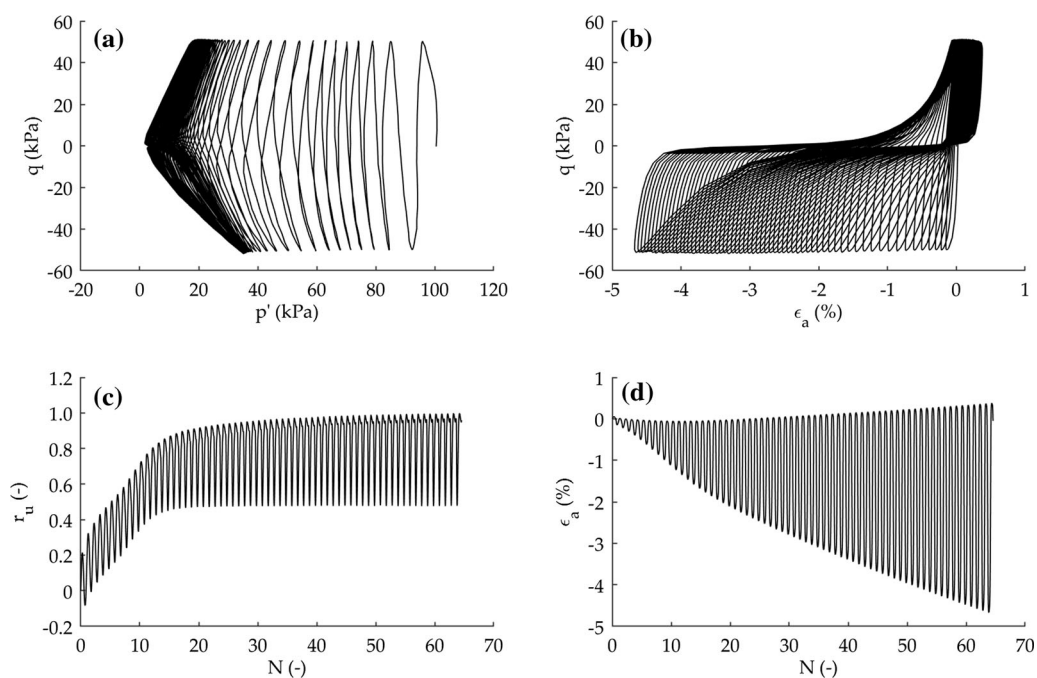**Fig. 4** Undrained response of untreated sand ($D_r = 29\%$; $CS_W = 0\%$; $CSR = 0.253$; $K_c = 1.0$; $p_0' = 100$ kPa)

**Fig. 5** Undrained response of stabilised sand ($D_r$ = 35%; $CS_W$ = 5%; $CSR$ = 0.253; $K_c$ = 1.0; $p_0'$ = 100 kPa)
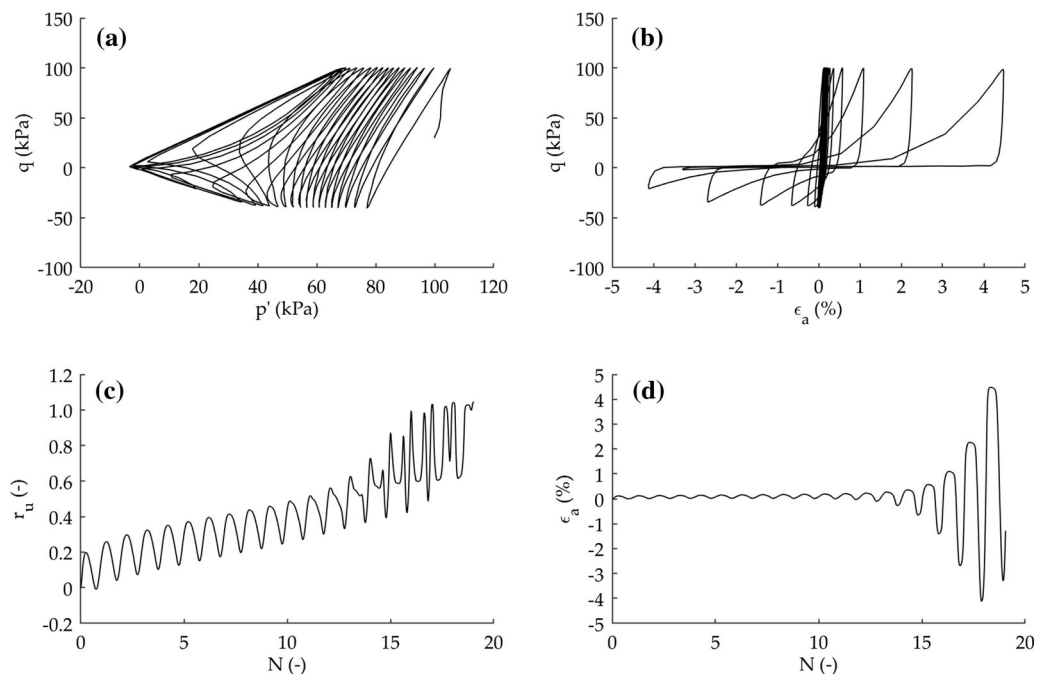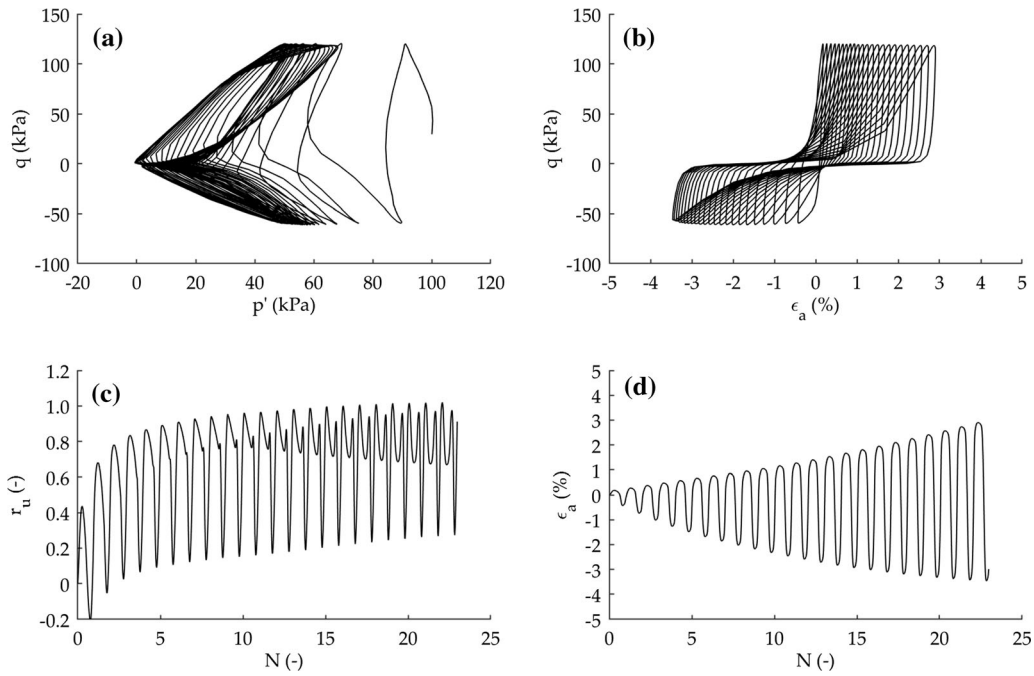


**Fig. 6** Undrained response of untreated sand ($D_r$ = 32%; $CS_W$ = 0%; $CSR$ = 0.352; $K_c$ = 1.3; $p_0'$ = 100 kPa)

comparing Figs. 4 and 5, it is shown that (under the same $CSR$) $N_f(CS_W = 5\%) > N_f(CS_W = 0\%)$, confirming the benefits of the CS treatment in improving the cyclic response of liquefiable sand.

### 3.2.2 Anisotropic initial stress conditions

Figures 6 and 7 show the results for $K_c$ = 1.3 on untreated sand and on stabilised sand, respectively. The applied cyclic deviatoric stress is different, resulting in $CSR$ = 0.352

**Fig. 7** Undrained response of stabilised sand ($D_r$ = 32%; $CS_W$ = 5%; $CSR$ = 0.460; $K_c$ = 1.3; $p_0'$ = 100 kPa)
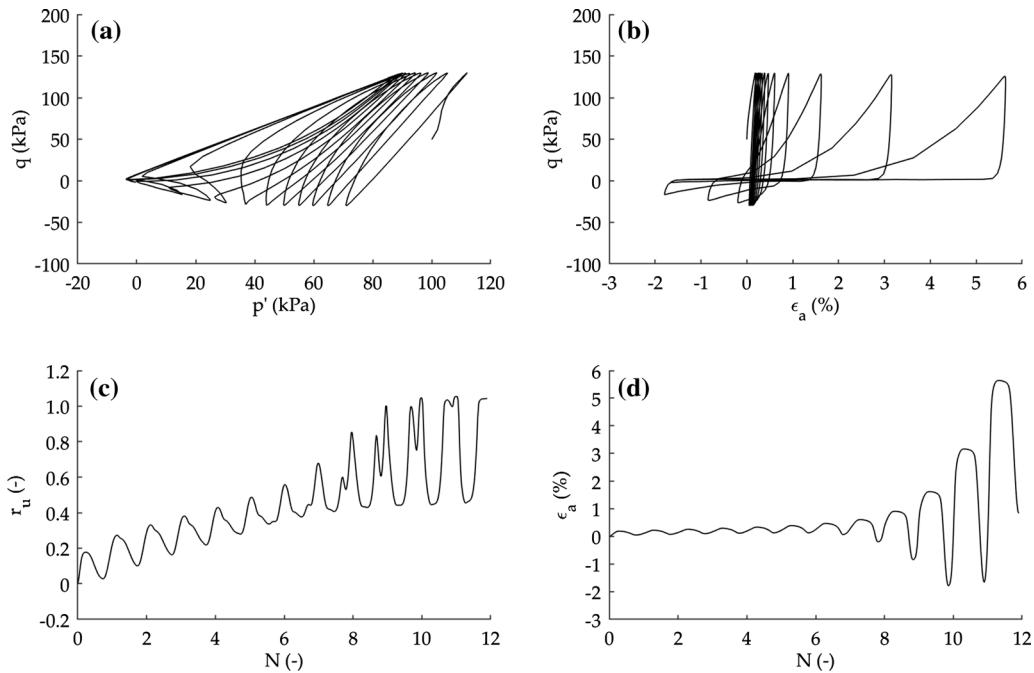


**Fig. 8** Undrained response of untreated sand ($D_r$ = 31%; $CS_W$ = 0%; $CSR$ = 0.401; $K_c$ = 1.6; $p_0'$ = 100 kPa)

(Fig. 6) and $CSR$ = 0.460 (Fig. 7) for untreated sand and for stabilised sand, respectively. For the untreated sand, the stress paths and deformation patterns are similar to those exhibited in the case of $K_c$ = 1.0 (Fig. 4). For the stabilised material (Fig. 7), it is worth observing that $r_u$ shows great amplitude oscillations within each loading cycle; the initial liquefaction condition is reached for $N$ = 16, and failure

occurs at $N_f$ = 17 ($\varepsilon_{DA}$ = 5.06%). Compared to the condition $K_c$ = 1.0 (Fig. 5), the axial strain is much more symmetrical about the zero-strain axis. By comparing Figs. 6 and 7 it should be noted that stabilised sand and untreated sand fail at a similar number of loading cycles ($N_f$ = 17 and $N_f$ = 18, respectively), although the applied cyclic stress
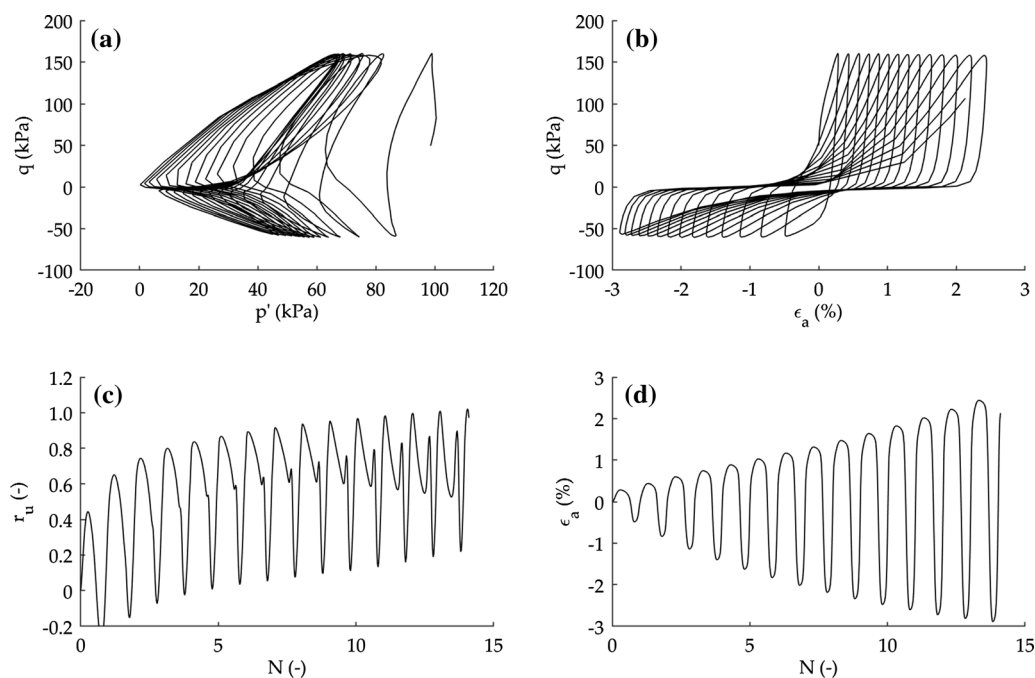
**Fig. 9** Undrained response of stabilised sand ($D_r$ = 31%; $CS_W$ = 5%; $CSR$ = 0.560; $K_c$ = 1.6; $p_0'$ = 100 kPa)

was significantly greater for the stabilised sand than for the untreated one.

Broadly speaking, by comparing the $N_f$ values for similar $CSR$ values in the cases of $K_c$ = 1.0–1.3 on untreated sand (Table 1), it follows that the presence of a static shear stress improves the cyclic response of the anisotropically consolidated material: by way of example, the failure condition was reached for $N_f$ = 4 under $CSR$ = 0.303 with $K_c$ = 1.0 and for $N_f$ = 57 under $CSR$ = 0.301 with $K_c$ = 1.3. The same holds for the stabilised sand specimens: by way of example, the failure condition was reached for $N_f$ = 13 under $CSR$ = 0.302 (the maximum $CSR$ adopted for tests on stabilised sand in isotropic state, series 1, Table 1) with $K_c$ = 1.0, and for $N_f$ = 58 under $CSR$ = 0.362 (the minimum $CSR$ adopted for tests on stabilised sand in $K_c$ = 1.3 condition, series 2, Table 1) with $K_c$ = 1.3.

Figures 8 and 9 show the results for $K_c$ = 1.6. In this case, the untreated sand specimen fails in 12 cycles under $CSR$ = 0.401 (Fig. 8), while the stabilised one fails in 13 cycles under $CSR$ = 0.560 (Fig. 9). The $r_u$ amplitude oscillations increased with increasing $K_c$ from 1.0 to 1.6 (Figs. 5c, 7c, 9c).

### 3.2.3 General comments

In none of the experimental tests performed in this study on sand stabilised by CS the $r_u$ = 1.0 condition represented a state of softening in the same way it was for the untreated

soil: the stabilised material could be stressed by many more loading cycles after the $r_u$ = 1.0 condition, and no sudden axial strain increase was detected afterwards. In stabilised sand, the axial strain progressively and steadily increased with the number of loading cycles. On untreated sand in the isotropic state, the condition $r_u$ = 1.0 was immediately followed by the development of $\varepsilon_{DA} \geq 5\%$. Conversely, when $K_c$ = 1.6, some additional loading cycles after $r_u$ = 1.0 were required to achieve $\varepsilon_{DA} \geq 5\%$. When $K_c$ = 1.3, $\varepsilon_{DA} \geq 5\%$ was either achieved a few cycles after $r_u$ = 1.0 or immediately following the initial liquefaction condition. On stabilised sand, instead, when $K_c$ = 1.0 the $r_u$ = 1.0 condition was reached earlier than the achievement of $\varepsilon_{DA} \geq 5\%$; the contrary happened for 1/4 tests for $K_c$ = 1.3 and for 3/4 tests $K_c$ = 1.6. It seems reasonable to expect that, for further increase of $K_c$ values in stabilised sand, the failure condition in terms of DA axial strain would always anticipate the $r_u$ = 1.0 condition. It is clear, however, that the failure mechanism in stabilised sand is mainly due to fatigue phenomena, depending on the CS bonding degradation during cyclic loading, rather than to the pore water pressure build-up.

### 3.3 Cyclic resistance

Figure 10 shows the liquefaction resistance curves in $N_f$-$CSR$ plane for all tests performed in this study, obtained via a power regression of experimental $N_f$-$CSR$ data. It is shown that the cyclic behaviour of sand is improved as
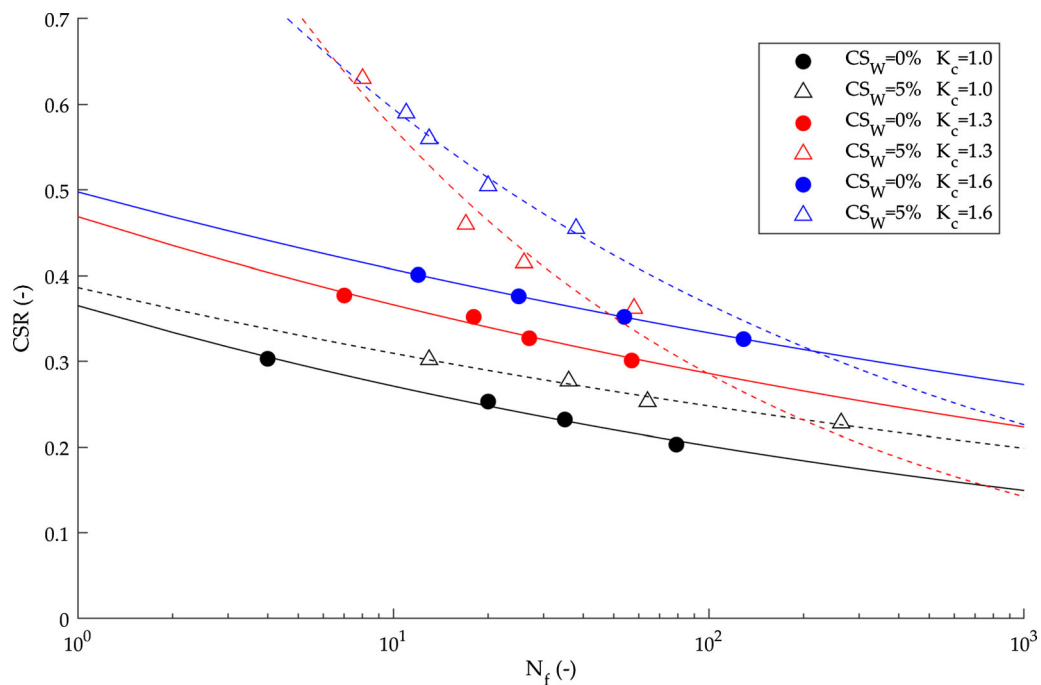
**Fig. 10** Number of loading cycles at failure against cyclic stress ratio for untreated sand (solid lines) and stabilised sand (dashed lines)

both $CS_W$ and $K_c$ values increase. For the untreated sand, the cyclic resistance curves are almost parallel in the $N_f$-$CSR$ plane, laying one above the other as $K_c$ increases. This also holds for the stabilised sand, for which the $K_c$ increase seems to induce a significant change in the steepness of the cyclic resistance curve. This effect is much more pronounced for $K_c = 1.3$ than for $K_c = 1.6$, if compared to the condition $K_c = 1.0$. With reference to the mean value of the number of equivalent stress cycles for a 7.5 magnitude earthquake [36], $N_{eq} = 15$, the cyclic resistance ratio at $N_f = 15$, $CRR_{15}$, was calculated on each cyclic resistance curve, and it corresponds to the $CSR$ value required to produce failure in 15 loading cycles. The influence of $K_c$ on $CRR_{15}$ is shown in Fig. 11. For the testing conditions used in this study, it was found that increasing $K_c$ was always beneficial in increasing $CRR_{15}$ for both stabilised sand and untreated sand. Figure 12 shows $N_f$ against $CSR* = CSR/K_c$, where $CSR*$ is the equivalent cyclic stress ratio needed to induce failure in $N_f$ cycles, as if all the specimens were in the condition $K_c = 1.0$. With this assumption, two different series can be identified, one for the stabilised material and one for the untreated one. As shown in Fig. 12, the experimental data can be interpolated by two distinct curves, confirming that the liquefaction resistance curve is higher for stabilised sand than for untreated one, regardless of the initial degree of anisotropy.

## 3.4 Axial strain and pore pressure development

In this paper, the axial strain developed during cyclic loading was used to identify the failure condition on a common basis. However, as shown in representative plots for both materials (untreated and stabilised, Figs. 4, 5, 6, 7, 8, 9), the way both the axial strain and the pore pressure build-up develop shows distinctive features depending on $CS_W$. For this reason, both the axial strain and the pore water pressure response are more in-depth analysed in the following Sections.

### 3.4.1 Axial strain

Figure 13 shows, for the untreated sand, the ratio $N/N_f$ versus the strain ratio $\varepsilon_{DA}/\varepsilon_{DA,f}$ (calculated within each loading cycle), for $K_c = 1.0$ (Fig. 13a), $K_c = 1.3$ (Fig. 13b), $K_c = 1.6$ (Fig. 13c); Fig. 13d shows a summary plot on tests subjected to similar $CSR$ values with varying $K_c$. As shown in Fig. 13a, the ratio $\varepsilon_{DA}/\varepsilon_{DA,f}$ slightly increases until $N/N_f \approx 0.8$ for tests subjected to $CSR = 0.203$–$0.253$, and it sharply increases afterwards; furthermore, for a given $N/N_f$, $\varepsilon_{DA}/\varepsilon_{DA,f}$ increases with $CSR$. When the applied $CSR$ is high enough to induce in the specimen a state of instability from the early loading cycles, the amount of $\varepsilon_{DA}/\varepsilon_{DA,f}$ is also significant for lower $N/N_f$ values, and the curve is smoother: the specimen subjected to $CSR = 0.303$ failed at $N_f = 4$.
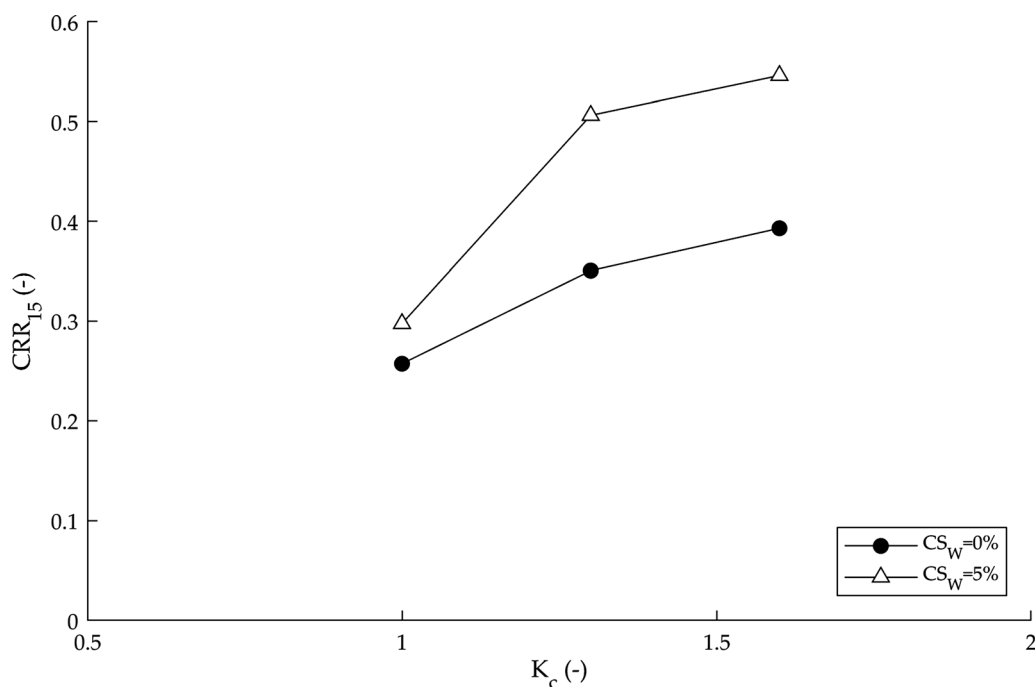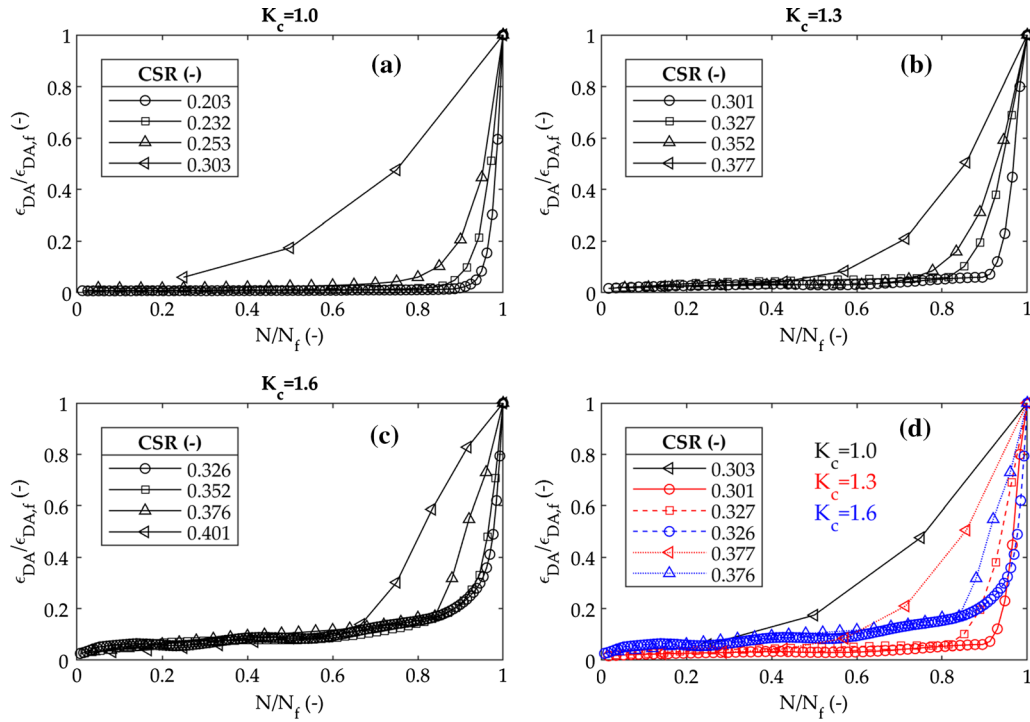
**Fig. 13** Number of loading cycles to the number of loading cycles at failure versus DA axial strain to the DA axial strain at failure for untreated sand: **a** $K_c = 1.0$, **b** $K_c = 1.3$, **c** $K_c = 1.6$, and **d** summary of tests under similar *CSR* values
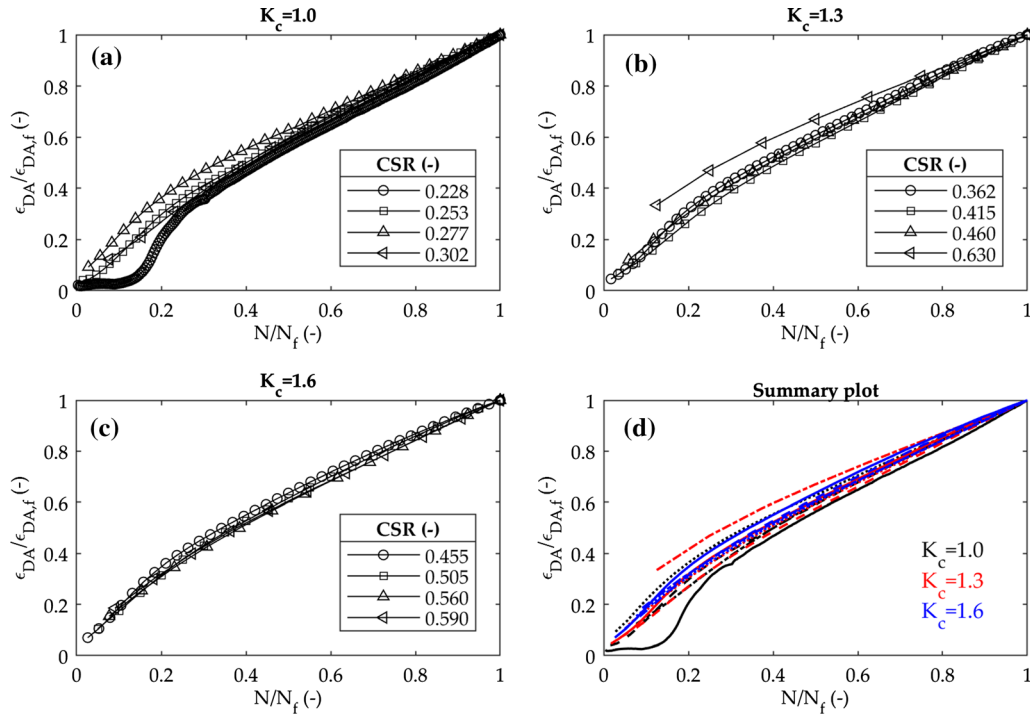


**Fig. 14** Number of loading cycles to the number of loading cycles at failure versus DA axial strain to the DA axial strain at failure for stabilised sand: **a** $K_c = 1.0$, **b** $K_c = 1.3$, **c** $K_c = 1.6$, and **d** summary of all tests

summary plot of all tests with varying $K_c$. The strain ratio develops progressively without any abrupt curvature change before failure is reached (Fig. 14a–c); the shape of

the $\varepsilon_{DA}/\varepsilon_{DA,f}$ curves and their position in the $N/N_f$–$\varepsilon_{DA}/\varepsilon_{DA,f}$ plane is similar for almost all tests and in a narrow range of $\varepsilon_{DA}/\varepsilon_{DA,f}$ values (Fig. 14d). Contrary to what observed for

the untreated sand, the $\varepsilon_{DA}/\varepsilon_{DA,f}$ curves do not significantly depend on $CSR$ and $K_c$ (Fig. 14). Some of the curves show an initial shape with a double inflection point for $N/N_f < 0.2$; this is well observed for those specimens whose failure condition was achieved after numerous loading cycles. This experimental evidence is associated with the lowest $CSR$ values adopted in each test series shown in Table 1 ($CSR = 0.228$, Fig. 14a; $CSR = 0.362$, Fig. 14b; $CSR = 0.455$, Fig. 14c). It is not clear whether a sort of yielding point exists (or becomes evident) under certain conditions. From the test configurations and results, Fig. 14d shows that the increase rate of the strain ratio is fairly constant in stabilised sand; a faster rate of increase was found in the range $N/N_f < 0.3$ for approximately all tests.

Furthermore, it is shown in Figs. 13 and 14 that the strain ratio builds up faster in stabilised soil than in the untreated one. The initial stiffness of sand samples stabilised by CS, which is lower than that of untreated sand samples (as observed in cyclic and monotonic loading conditions [2, 29]), is responsible for the observed behaviour. For instance, $\varepsilon_{DA}/\varepsilon_{DA,f} \approx 0.6$ was achieved at $N/N_f \approx 0.8$ for an untreated sand sample under $CSR = 0.303$ (Fig. 13a); for a stabilised sand sample under similar testing conditions ($CSR = 0.302$, $K_c = 1$, Fig. 14a), $\varepsilon_{DA}/\varepsilon_{DA,f} \approx 0.6$ was obtained for $N/N_f \approx 0.45$. Nonetheless, the number of loading cycles at failure is higher for the stabilised sand than for the untreated one ($N_f = 13$ and $N_f = 4$, respectively, see Table 1).

### 3.4.2 Pore pressure

The extra pore water pressure generated during undrained cyclic loading consists of two components, transient and residual [18]: the former reflects the real-time change of applied total cyclic stress, whereas the latter is obtained at the end of each loading cycle, and it directly affects the effective stress of soil. For this reason, to investigate the pore water pressure response and its effects, it is convenient to refer to the residual pore water pressure ratio, here indicated as $RPWP$.

As shown in Sect. 3.2, the extra pore water pressure in untreated samples progressively builds up, eventually approaching $p_0'$. Figure 15 shows $N/N_f$ versus $RPWP$ for untreated sand with varying $K_c$ (Fig. 15a–c) and a summary plot of tests with similar $CSR$ (Fig. 15d). The shape of the $N/N_f$-$RPWP$ curves is typical of clean sands [38]; in this case, the $RPWP$ development can be quite satisfactorily predicted by using empirical correlations already available in literature. The $RPWP$ curves, as well as strain ratio curves (Sect. 3.4.1), depend both on $CSR$ (Fig. 15a–c) and on $K_c$ (Fig. 15d). For a given $K_c$, the $RPWP$ grows slower as $CSR$ decreases, except for the test under $CSR = 0.253$ (Fig. 15a–c), and the curves move downward in the $N/N_f$-$RPWP$ plane with increasing $K_c$ under a similar $CSR$ (Fig. 15d).

In stabilised sand, the extra pore water pressure builds up faster than in the untreated soil (Sect. 3.2), accordingly with previous observations and pore water pressure measurements in materials stabilised by CS [29, 31]. Figure 16 shows $N/N_f$ versus $RPWP$ for stabilised sand with varying $K_c$ (Fig. 16a–c) and a summary plot of all tests (Fig. 16d). The way $RPWP$ develops resembles typical trends shown in cemented or moderately cemented sands [5, 33, 53]. Test results do not show a clear dependence of the relationship $N/N_f$-$RPWP$ on the applied $CSR$ (Fig. 16a–c), nor on $K_c$ (Fig. 16d).

Porcino et al. [33] proposed a 4-parameter model to describe the $RPWP$ trends in specimens stabilised with a mineral-based grout and subjected to cyclic simple shear tests. According to [33], the model parameters mainly depend on the type and level of cementation, and on $D_r$. Based on the experimental results obtained from cyclic triaxial tests on stabilised sand samples (Fig. 16), the following 3-parameter equation is here proposed to describe the $RPWP$ development:

$$RPWP = 1 - 1/\left(1 + m\frac{N}{N_f}\right)^n \qquad (3)$$

In Eq. 3, $m$, $n$, $N_f$ are the model parameters to be calibrated on the experimental data. The parameters $m$ and $n$ in Eq. 3 are related to each other by a power function, as shown in Fig. 17, so that Eq. 3 can be rewritten as follows:

$$RPWP = 1 - 1/\left(1 + m\frac{N}{N_f}\right)^{7.379m^{-0.947}} \qquad (4)$$

Figure 18 shows the fitting of the proposed models (Eqs. 3 and 4) on 2 tests on stabilised sand, characterised by similar $CSR$ and different $K_c$ values (ID 07-5, ID 09-5). As expected, Eq. 3 is more accurate than Eq. 4 in data fitting, being the latter less able to predict the RPWP development especially for $N/N_f < 0.3$. However, Eq. 4 requires less calibration parameters, and it could ultimately be a satisfactory compromise, considering that the pore pressure build-up is not a significant indicator of the collapse in stabilised sand. It should be noted that none of the proposed models can satisfactorily match the behaviour observed in case of $K_c = 1$ and $CSR = 0.228$ for $0 < N/N_f \approx < 0.2$ (Fig. 16a), and, more in general, the behaviour observed when the applied $CSR$ was so low that a large number of loading cycles were required to achieve failure.
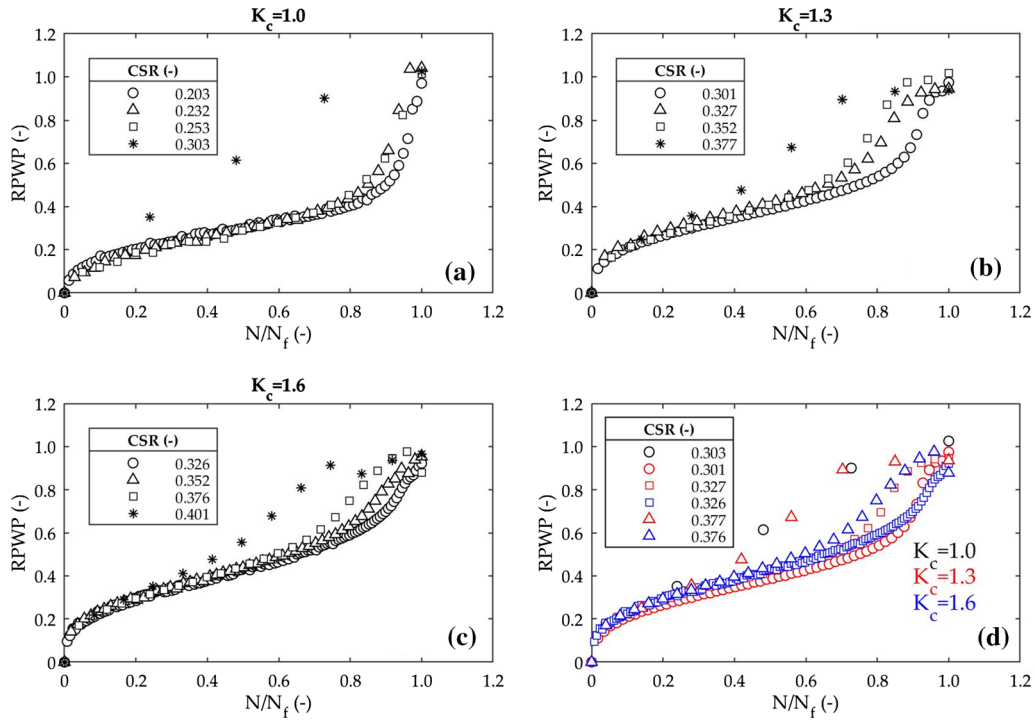
**Fig. 15** Number of loading cycles to the number of loading cycles at failure versus residual pore water pressure for untreated sand: **a** $K_c$ = 1.0, **b** $K_c$ = 1.3, **c** $K_c$ = 1.6, and **d** summary of tests under similar *CSR* values
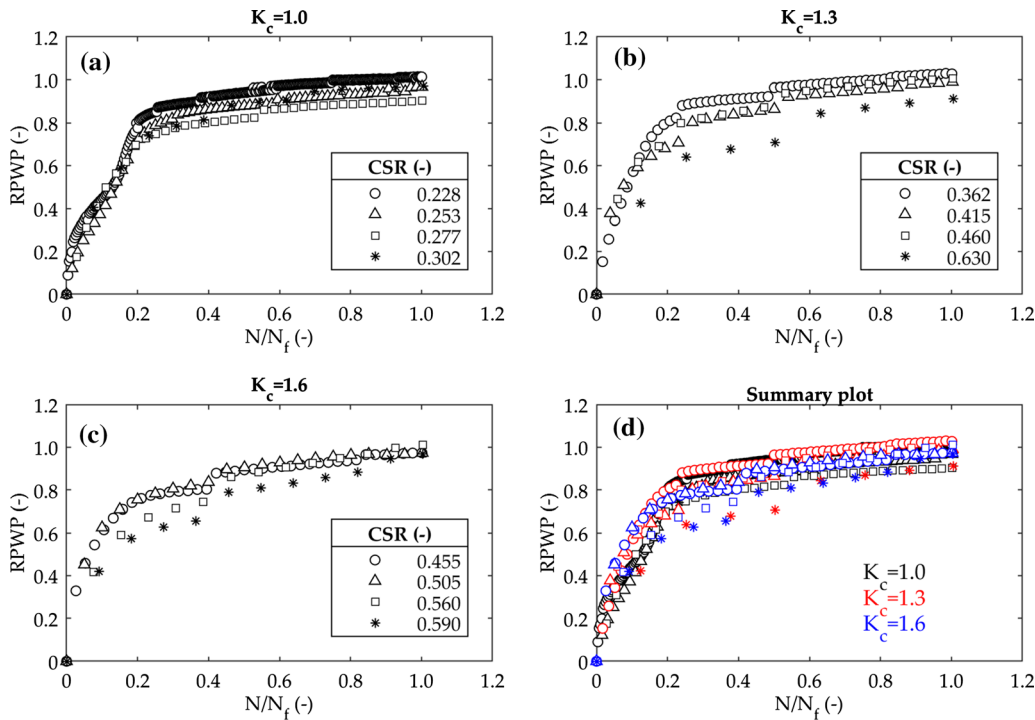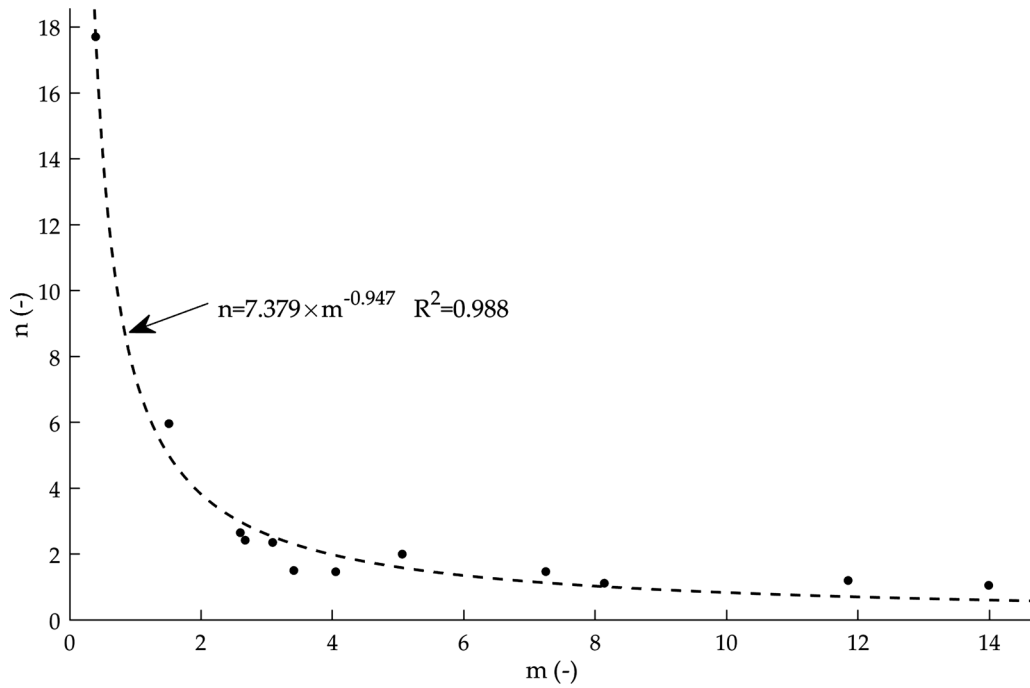


**Fig. 16** Number of loading cycles to the number of loading cycles at failure versus residual pore water pressure for stabilised sand: **a** $K_c$ = 1.0, **b** $K_c$ = 1.3, **c** $K_c$ = 1.6, and **d** summary of all tests

**Fig. 17** Relationship between parameters $m$, $n$ obtained from experimental data
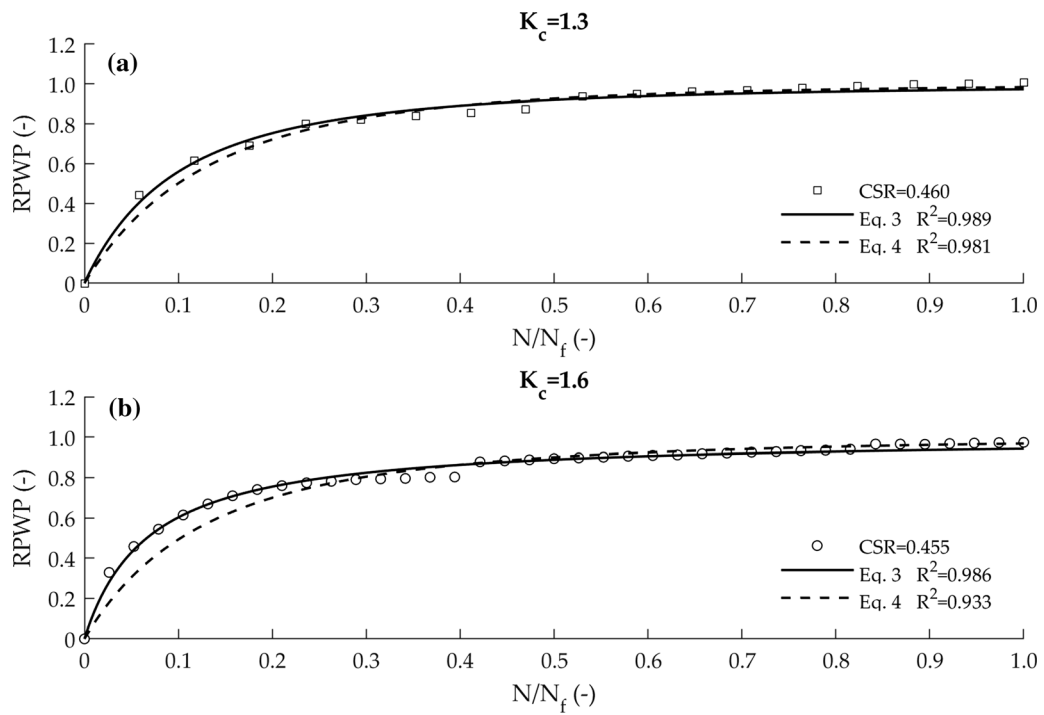


**Fig. 18** Curve fitting of the proposed models (Eqs. 3 and 4) on experimental data: **a** ID 07-5, **b** ID 09-5

## 4 Conclusions

Undrained cyclic triaxial tests were performed on loose untreated sand samples and on loose sand samples stabilised by colloidal silica (CS). All samples were subjected to isotropic or anisotropic consolidation, to investigate the influence of an initial static shear stress on the cyclic response of the materials. The behaviour during the consolidation process, the deformation patterns, the cyclic resistance and the pore water pressure generation under cyclic loading were analysed. Based on the experimental findings of this study, the following conclusions can be drawn.

- Under isotropic consolidation, pore water pressure dissipation and volumetric strain development are almost immediate for the untreated sand; both phenomena are instead delayed for the stabilised one.
- The stabilised soil is more compressible than the untreated one under the same initial conditions, showing greater maximum volumetric strain during the isotropic consolidation process.
- Simple models are proposed to fit the curves of the volumetric strain variation and of the average consolidation ratio (in terms of pore water pressure dissipation) for the stabilised soil during isotropic consolidation in triaxial tests.
- The stress paths and deformations patterns resulting from cyclic triaxial tests are significantly different and distinctive for stabilised sand and for the untreated one, for all investigated initial stress conditions (isotropic or anisotropic, with the consolidation stress ratio $K_c$ (the ratio between axial and radial effective stresses) equal to 1.0, 1.3 and 1.6). For the untreated sand, the initial liquefaction is a state of softening that anticipates the sudden development of significant axial strain amount, leading the soil to collapse. For the stabilised sand, the axial strain progressively accumulates during loading: the initial liquefaction condition is not representative of the specimens' collapse.
- The rate at which the extra pore water pressure increases during cyclic loading is higher for stabilised sand than for untreated sand.
- The cyclic resistance of sand stabilised by CS is higher than that of the untreated one. The cyclic resistance increases as $K_c$ increases for both stabilised sand and untreated sand specimens.
- For the untreated sand, the ratio of the double amplitude axial strain to the double amplitude axial strain at failure (strain ratio) clearly depends on the applied cyclic stress ratio (CSR) and $K_c$. On the contrary, for the stabilised soil, the strain ratio increases without showing any clear dependence on CSR and $K_c$. Moreover, the strain ratio builds up faster in stabilised soil.
- The shape of the residual pore water pressure ratio (RPWP) curves resembles that of clean sand and lightly cemented sand, for untreated sand and stabilised sand, respectively.
- RPWP clearly depends on $K_c$ and CSR for the untreated sand, while the same does not hold for the stabilised sand.
- A parametric model fitting the experimental data for RPWP development in stabilised sand is proposed.

**Data availability** All data that support the findings of this study are available from the corresponding author upon reasonable request.

## References

1. Agapoulaki GI, Papadimitriou AG (2018) Rheological properties of colloidal silica grout for passive stabilization against liquefaction. J Mat Civ Eng. https://doi.org/10.1061/(ASCE)MT.1943-5533.0002377

2. Ciardi G, Bardotti R, Vannucchi G, Madiai C (2019) Effects of high-diluted colloidal silica grout on the mechanical behavior of a liquefiable sand. In: Proceedings of the 7th international conference on earthquake geotechnical engineering, Roma, IT, pp 1820–1827

3. Ciardi G, Bardotti R, Vannucchi G, Madiai C (2020) Effects of high-diluted colloidal silica grouting on the behaviour of a liquefiable sand. Geotech Res. https://doi.org/10.1680/jgere.20.00010

4. Ciardi G, Vannucchi G, Madiai C (2021) Effects of colloidal silica grouting on geotechnical properties of liquefiable soils: a review. Geotechnics. https://doi.org/10.3390/geotechnics1020022

5. Clough GW, Iwabuchi J, Rad NS, Kuppusamy T (1989) Influence of cementation on liquefaction of sands. J Geotech Eng 115(8):1102–1117

6. Díaz-Rodríguez JA, Antonio-Izarraras VM, Bandini P, López-Molina JA (2008) Cyclic strength of a natural liquefiable sand

stabilized with colloidal silica grout. Can Geotech J. https://doi.org/10.1139/T08-072

7. DIN (Deutsches Institut für Normung) (1996) DIN 18126: soil, investigation and testing—determination of density of non-cohesive soils for maximum and minimum compactness. DIN, Berlin, Germany (**in German**)

8. Gallagher PM (2000) Passive site remediation for mitigation of liquefaction risk. PhD dissertation, Virginia Polytechnic Institute and State University, Blacksburg, VA, USA

9. Gallagher PM, Conlee CT, Rollins KM (2007) Full-scale field testing of colloidal silica grouting for mitigation of liquefaction risk. J Geotech Geoenv Eng. https://doi.org/10.1061/(ASCE)1090-0241(2007)133:2(186)

10. Gallagher PM, Lin Y (2009) Colloidal silica transport through liquefiable porous media. J Geotech Geoenv Eng. https://doi.org/10.1061/(ASCE)GT.1943-5606.0000123

11. Gallagher PM, Mitchell JK (2002) Influence of colloidal silica grout on liquefaction potential and cyclic undrained behavior of loose sand. Soil Dyn Earthq Eng. https://doi.org/10.1016/S0267-7261(02)00126-4

12. Gallagher PM, Pamuk A, Abdoun T (2007) Stabilization of liquefiable soils using colloidal silica grout. J Mat Civ Eng. https://doi.org/10.1061/(ASCE)0899-1561(2007)19:1(33)

13. Georgiannou VN, Pavlopoulou EM, Bikos Z (2017) Mechanical behaviour of sand stabilised with colloidal silica. Geotech Res. https://doi.org/10.1680/jgere.16.00017

14. Huang Y, Wang L (2016) Experimental studies on nanomaterials for soil improvement: a review. Environ Earth Sci. https://doi.org/10.1007/s12665-015-5118-8

15. Hyodo M, Tanimizu H, Yasufuku N, Murata H (1994) Undrained cyclic and monotonic triaxial behaviour of saturated loose sand. Soils Found. https://doi.org/10.3208/sandf1972.34.19

16. Idriss IM, Boulanger RW (2008) Soil liquefaction during earthquakes. Earthquake Engineering Research Institute, CA, US

17. Iler RK (1979) The chemistry of silica: solubility, polymerization, colloid and surface properties, and biochemistry. Wiley, New York

18. Ishibashi I, Sherif MA, Tsuchiya C (1977) Pore-pressure rise mechanism and soil liquefaction. Soils Found. https://doi.org/10.3208/sandf1972.17.2_17

19. Ishihara K (1993) Liquefaction and flow failure during earthquakes. Géotechnique. https://doi.org/10.1680/geot.1993.43.3.351

20. Karol RH (2003) Chemical grouting and soil stabilization, revised and expanded. CRC Press, Revised and Expanded

21. Kodaka T, Ohno Y, Takyu T (2005) Cyclic shear characteristics of treated sand with colloidal silica grout. In: Proceedings of the 16th international conference on soil mechanics and geotechnical engineering, pp 401–404

22. Kramer SL (1996) Geotechnical earthquake engineering. Prentice Hall, New York

23. Kuerbis R, Vaid YP (1988) Sand sample preparation—the slurry deposition method. Soils Found. https://doi.org/10.3208/sandf1972.28.4_107

24. Ladd RS (1978) Preparing test specimens using undercompaction. Geotech Test J 1(1):16–23

25. Mohamad R, Dobry R (1986) undrained monotonic and cyclic triaxial strength of sand. J Geotech Eng. https://doi.org/10.1061/(ASCE)0733-9410(1986)112:10(941)

26. Mollamahmutoglu M, Yilmaz Y (2010) Pre- and post-cyclic loading strength of silica-grouted sand. Proc Inst Civ Eng Geotech Eng. https://doi.org/10.1680/geng.2010.163.6.343

27. Mulilis JP, Seed HB, Chan CK, Mitchell JK, Arulanandan K (1977) Effects of sample preparation on sand liquefaction. J Geotech Eng Div. https://doi.org/10.1061/AJGEB6.0000387

28. Pan K, Yang ZX (2018) Effects of initial static shear on cyclic resistance and pore pressure generation of saturated sand. Acta Geotech. https://doi.org/10.1007/s11440-017-0614-5

29. Pavlopoulou EM, Georgiannou VN (2021) Effect of colloidal silica aqueous gel on the monotonic and cyclic response of sands. J Geotech Geoenv Eng. https://doi.org/10.1061/(ASCE)GT.1943-5606.0002641

30. Persoff P, Apps J, Moridis G, Whang JM (1999) Effect of dilution and contaminants on sand grouted with colloidal silica. J Geotech Geoenv Eng. https://doi.org/10.1061/(ASCE)1090-0241(1999)125:6(461)

31. Porcino D, Marcianò V, Granata R (2011) Undrained cyclic response of a silicate-grouted sand for liquefaction mitigation purposes. Geomechanics and Geoengineering. https://doi.org/10.1080/17486025.2011.560287

32. Porcino D, Marcianò V, Granata R (2012) Static and dynamic properties of a lightly cemented silicate-grouted sand. Can Geotech J. https://doi.org/10.1139/t2012-069

33. Porcino D, Marcianò V, Granata R (2015) Cyclic liquefaction behaviour of a moderately cemented grouted sand under repeated loading. Soil Dyn Earthq Eng. https://doi.org/10.1016/j.soildyn.2015.08.006

34. Rasouli R, Hayashi K, Zen K (2016) Controlled permeation grouting method for mitigation of liquefaction. J Geotech Geoenv Eng. https://doi.org/10.1061/(ASCE)GT.1943-5606.0001532

35. Salvatore E, Modoni G, Mascolo MC, Grassi D, Spagnoli G (2020) Experimental evidence of the effectiveness and applicability of colloidal nanosilica grouting for liquefaction mitigation. J Geotech Geoenv Eng. https://doi.org/10.1061/(ASCE)GT.1943-5606.0002346

36. Seed HB, Idriss IM, Makdisi F, Banerjee N (1975) Representation of irregular stress time histories by equivalent uniform stress series in liquefaction analyses. Earthquake Engineering Research Center (EERC), University of California, Berkeley, US, Report 75-29

37. Seed HB, Lee KL (1966) Liquefaction of saturated sands during cyclic loading. J Soil Mech Found Div 92(SM6):105–134

38. Seed HB, Martin PP, Lysmer J (1975) The Generation and Dissipation of Pore Water Pressures During Soil Liquefaction. Earthquake Engineering Research Center (EERC), University of California, Berkeley, US, Report 75-26

39. Sivathayalan S, Vaid YP (2002) Influence of generalized initial state and principal stress rotation on the undrained response of sands. Can Geotechl J. https://doi.org/10.1139/t01-078

40. Sögaard C, Funehag J, Abbas Z (2018) Silica sol as grouting material: a physio-chemical analysis. Nano Convergence. https://doi.org/10.1186/s40580-018-0138-1

41. Sze HY, Yang J (2014) Failure modes of sand in undrained cyclic loading: impact of sample preparation. J Geotech Geoenv Eng. https://doi.org/10.1061/(ASCE)GT.1943-5606.0000971

42. Towhata I (2008) Geotechnical earthquake engineering. Springer-Verlag, Berlin

43. Towhata I, Kabashima Y (2001) Mitigation of seismically-induced deformation of loose sandy foundation by uniform permeation grouting. In: Proceedings of the earthquake geotechnical engineering satellite conference, XVth international conference on soil mechanics and geotechnical engineering, Istanbul, TR, pp. 313–318

44. Triantafyllos PK, Georgiannou VN, Pavlopoulou EM, Dafalias YF (2021) Strength and dilatancy of sand before and after stabilisation with colloidal-silica gel. Géotechnique. https://doi.org/10.1680/jgeot.19.P.123

45. Vaid YP, Chern JC (1983) Effect of static shear on resistance to liquefaction. Soils Found. https://doi.org/10.3208/sandf1972.23.47

46. Vranna A, Tika T (2019) Laboratory improvement of liquefiable sand via colloidal silica and weak cementation. Proc Inst Civ Eng Ground Improv. https://doi.org/10.1680/jgrim.19.00019

47. Vranna A, Tika T, Papadimitriou A (2020) Laboratory investigation into the monotonic and cyclic behaviour of a clean sand stabilised with colloidal silica. Géotechnique. https://doi.org/10.1680/jgeot.18.P.213

48. Wang S, Luna R, Stephenson RW (2011) A slurry consolidation approach to reconstitute low-plasticity silt specimens for laboratory triaxial testing. Geotech Test J 34(4):288–296

49. Wei X, Yang J (2019) Cyclic behavior and liquefaction resistance of silty sands with presence of initial static shear stress. Soil Dyn Earth Eng. https://doi.org/10.1016/j.soildyn.2018.11.029

50. Whang JM (1995) Assessment of Barrier Containment Technologies for Environmental Remediation Applications. In: Rumer RR, Mitchell JK (eds) Chemical-based barrier materials. National Technical Information Service, Springfield, VA, US, Section 9, pp 211–247

51. Wichtmann T, Triantafyllidis T (2016) An experimental database for the development, calibration and verification of constitutive models for sand with focus to cyclic loading: part I—tests with monotonic loading and stress cycles. Acta Geot. https://doi.org/10.1007/s11440-015-0402-z

52. Wong C, Pedrotti M, El Mountassir G, Lunn RJ (2018) A study on the mechanical interaction between soil and colloidal silica gel for ground improvement. Eng Geol. https://doi.org/10.1016/j.enggeo.2018.06.011

53. Xiao P, Liu H, Xiao Y, Stuedlein AW, Evans TM (2018) Liquefaction resistance of bio-cemented calcareous sand. Soil Dyn Earthq Eng 107:9–19

54. Yang J, Sze HY (2011) Cyclic behaviour and resistance of saturated sand under non-symmetrical loading conditions. Géotechnique. https://doi.org/10.1680/geot.9.P.019

55. Yang J, Sze HY (2011) Cyclic strength of sand under sustained shear stress. J Geotech Geoenv Eng. https://doi.org/10.1061/(ASCE)GT.1943-5606.0000541

56. Yang ZX, Li XS, Yang J (2008) Quantifying and modelling fabric anisotropy of granular soils. Géotechnique. https://doi.org/10.1680/geot.2008.58.4.237

57. Yang ZX, Pan K (2017) Flow deformation and cyclic resistance of saturated loose sand considering initial static shear effect. Soil Dyn Earthq Eng. https://doi.org/10.1016/j.soildyn.2016.09.002

58. Yang ZX, Pan K (2018) Energy-based approach to quantify cyclic resistance and pore pressure generation in anisotropically consolidated sand. J Mater Civ Eng. https://doi.org/10.1061/(ASCE)MT.1943-5533.0002419

59. Yonekura R, Miwa M (1993) Fundamental properties of sodium silicate based grout. In: Proceedings of the eleventh Southeast Asian geotechnical conference, Singapore, pp 439–444

60. Yoshimi Y, Oh-Oka H (1975) Influence of degree of shear stress reversal on the liquefaction potential of saturated sand. Soils Found. https://doi.org/10.3208/sandf1972.15.3_27